WILEY-VCH

Edited by
Chunnian He, Naiqin Zhao, and Junwei Sha

Templated Fabrication of Graphene-Based Materials for Energy Applications

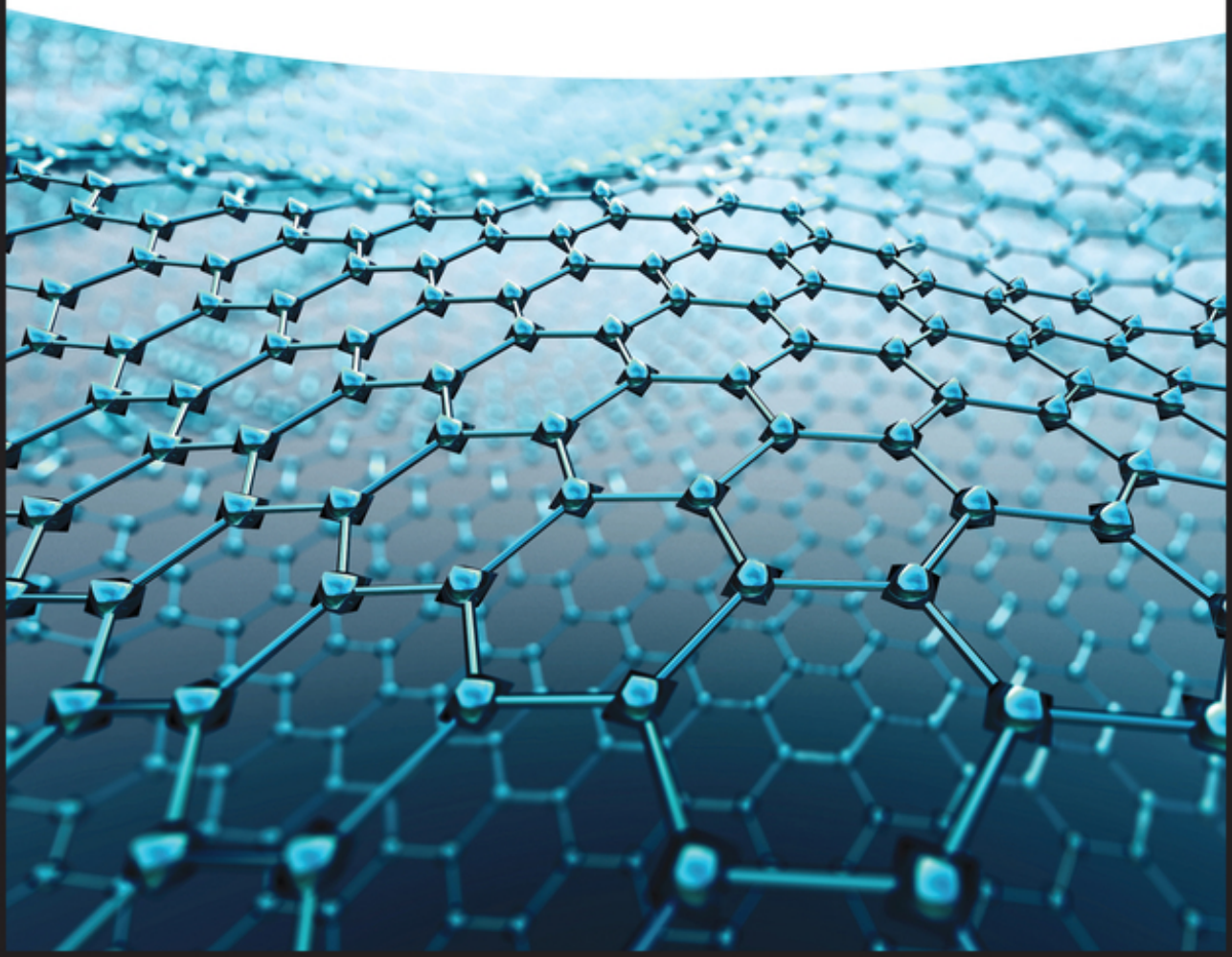

Templated Fabrication of Graphene-Based Materials for Energy Applications

Templated Fabrication of Graphene-Based Materials for Energy Applications

Edited by

Chunnian He, Naiqin Zhao, and Junwei Sha

WILEY-VCH

Editors

Prof. Chunnian He
Tianjin University
Materials Science and Engineering
Peiyang Park Campus
No.135 Yaguan Road
Haihe Education Park
300350 Tianjin
China

Prof. Naiqin Zhao
Tianjin University
Materials Science and Engineering
Peiyang Park Campus
No.135 Yaguan Road
Haihe Education Park
300350 Tianjin
China

Assoc. Prof. Junwei Sha
Tianjin University
Materials Science and Engineering
Peiyang Park Campus
No.135 Yaguan Road
Haihe Education Park
300350 Tianjin
China

Cover Image: © Neon_dust/Shutterstock

Library of Congress Card No.: applied for

British Library Cataloguing-in-Publication Data
A catalogue record for this book is available from the British Library.

Bibliographic information published by the Deutsche Nationalbibliothek
The Deutsche Nationalbibliothek lists this publication in the Deutsche Nationalbibliografie; detailed bibliographic data are available on the Internet at <http://dnb.d-nb.de>.

Print ISBN: 978-3-527-34600-4
ePDF ISBN: 978-3-527-82209-6
ePub ISBN: 978-3-527-34625-7
oBook ISBN: 978-3-527-82208-9

Typesetting Straive, Chennai, India

Printed on acid-free paper

Contents

Preface

With carbon neutrality being raised as the high-priority mission for human society, there is an urgent need for technological development in related fields. In particular, the demand for energy storage and conversion applications, represented by batteries, is increasing rapidly. Moreover, their development of energy-related applications greatly boosted the requirements for new materials.

Among various new materials, graphene is undoubtedly the most popular one. Since its discovery, graphene has become a star material due to its excellent mechanical, electrical, and chemical properties. However, in energy-related fields such as batteries, supercapacitors, and electrocatalysis, the demand for materials has a different focus. How to manufacture and improve the graphene-based materials to meet different needs is a question worth exploring. Among the many strategies to prepare graphene-based materials, the template method is one of the most popular methods. The advantage of the template method is that it can effectively regulate the microstructure of graphene. Also, such a method can introduce heteroatoms or other phases in graphene by the interaction between the template and precursors during the preparation process. There are more and more researchers recognizing the benefits of the template method for graphene-based materials production. There has been a rapid growth in research in this area and many promising applications have emerged. Therefore, we think it is necessary to summarize and review the development in this field, which is the main reason why we have written this book.

The framework of this book can be broadly divided into three parts. Firstly, we will start with a basic introduction to graphene-based materials (Chapters 1 and 2); the second part is the frontier of template methods for the preparation of graphene-based materials (Chapters 3–5); the third part is the research progress of graphene-based materials in different energy-related applications (Chapter 6–10).

Chapter 1 mainly introduces the basic knowledge of graphene, including its history and physical properties. The purpose of this chapter is to give the reader a background for the following chapters. Chapter 2 will give readers a grasp of the current synthesis strategies for graphene. To this regard, the classification of graphene preparations is described and some typical researches are introduced in this chapter. Chapters 3 to 5 will focus on a brief overview of different kinds of template methods for graphene production. The study of porous metals for graphene preparation is presented in Chapter 3. Nanoporous graphene shows excellent physics and

electrochemical performance in the fields of energy storage and conversion due to its high-quality and unique interconnected structure. Chapter 3 presents an overview of the recent research about the nanoporous graphene-based materials using nanoporous metal as the substrates. Then, Chapter 4 focuses on how to prepare graphene in large quantities, in particular. Considering the cost of graphene preparation with the potential for a large number of applications, substantial efforts have been devoted to developing a facile and versatile method, and several low-cost template methods will be reviewed in this part. In Chapter 5, the strategy of powder metallurgy and additive manufacturing procedures to prepare graphene materials is highlighted, which is one of the current research interests of our group. Subsequent chapters will discuss the various applications of graphene-based materials, such as lithium-ion batteries (Chapter 6), lithium-metal batteries (Chapter 7), lithium-sulfur batteries (Chapter 8), supercapacitors (Chapter 9), electrocatalysis (Chapter 10), and so on. Chapters 6 to 10 all follow a similar framework of discussion. At first, we will give the background of these fields, such as the basic concepts in energy applications and the physicochemical principles for different devices. Then, the discussion of the current bottlenecks in materials encountered in these applications will be presented. Consequently, we will describe why graphene-based materials are promising in these fields and how graphene should be improved to suit the different requirements. Meanwhile, we will review the specific applications of graphene-based materials prepared by the template methods in these fields and give the properties that can be achieved or the performance in practical cases. At the end of each chapter, we will discuss the current challenges of these graphene-based materials in each energy-related application, as well as possible improvement strategies and directions.

In these chapters, relevant content includes both the authors' studies and the research of others. This content has been reorganized and reviewed to form systematic frameworks. It is my pleasure to write and edit this book on graphene-based materials and their energy applications. It is hoped that the publication of this book will be helpful to researchers in this field and provide guidelines for related researches. Special thanks go to my students, colleagues, and the publisher's editors for their discussions and help.

List of Abbreviations

0D	zero-dimensional
1D	one-dimensional
2D Fe_3O_4@C@PGC	2D porous graphitic carbon nanosheets uniformly embedded with carbon-encapsulated Fe_3O_4 nanoparticles
2D	two-dimensional
3D BMG	three-dimensional bi-functional modular graphene network
3D CG	3D graphene-based hosts with continuous ductlike structure
3D FL-MoS_2@PCNNs	few layers MoS_2 nanosheets anchored on 3D porous carbon nanosheet networks
3D G	3D graphene architectures
3D GF	3D graphene foam
3D GF-FeS_2	cauliflower-like FeS_2 anchored on three-dimensional graphene foams
3D GM	3D graphene monolith
3D GN	three-dimensional graphene foams
3D GNs	3D porous graphene-like networks
3D PG	3D porous graphene
3D Rebar GF	CNTs-reinforced 3D graphene foam
3D S@PGC	sulfur nanoparticles in three-dimensional (3D) porous graphitic carbon (PGC)
3D SnSb@N–PG	SnSb in-plane nanoconfined three-dimensional N-doped porous graphene composite microspheres
3D ZnO@PCCMs	ZnO nanoparticle-confined 3D porous carbon composite microspheres
3D	three-dimensional
3DCu@NG	nanoporous Cu@N-doped graphene
3D-DG	free-standing 3D duct-like graphene
3D-DG@MnO_2	3D nanoporous graphene @MnO_2 composite
ΔG	Gibbs free energy
AFM	atomic force microscopy
AGNRs	armchair graphene nanoribbons
ALD	atomic layer deposition
a-MEGO	KOH-activated microwave-exfoliated graphite oxide

a-MnO_x	amorphous manganese oxide
AMs	anode materials
An	aniline
APCVD	atmospheric-pressure CVD
APS	aminopropyltriethoxysilane
APTMS	3-aminopropyl-trimethoxysilane
ASCs	asymmetric supercapacitors
a-TiO_2	amorphous TiO_2
BET	Brunauer–Emmett–Teller
BF-STEM	bright-field scanning transmission electron microscopy
B-LIG-MSCs	flexible supercapacitors based on boron-doped laser scribing graphene
BN-GAs	nitrogen and boron co-doped monolithic graphene aerogels
C	capacitance
C60	fullerene
carbide@CNS	vertically aligned 2D N-doped carbon nanosheets embedded with uniform nanosized metal carbides
Cat	catecho
CE	coulombic efficiency
CNF	carbon nanofiber
CNFs	carbon nanofibers
CNs	carbon nanosheets
CNTs	carbon nanotubes
CO_2RR	carbon dioxide reduction reaction
Co_3O_4/GS	Co_3O_4/graphene sheets
Co-MOF/3DGN	Co-MOF/three-dimensional graphene network
CoS_2/G	CoS_2/graphene/CoS_2 heterostructure
CoS_2-N-C/3DGN	CoS_2 encapsulated in N-doped carbon/3DGN
CPD	critical point dryer
CS-800A	S-doped carbons synthesized from K_2SO_4 at 800 °C
CS–800B	S-doped carbons synthesized from $Na_2S_2O_3$ at 800 °C
CTAB	cetyltrimethylammonium bromide
CV	cyclic voltammogram
CVD	chemical vapor deposition
DA	dopamine hydrochloride
DFT	density functional theory
DMA	dynamic mechanical analysis
DOS	density-of-states
E	energy density
ECR	electrochemical CO_2 reduction
EDLCs	electrical double-layer capacitors
EELS	electron energy-loss spectroscopy
EIS	electrochemical impedance spectroscopy
EOG	edge-oriented multilayer graphene

Fe@C@PGC	2D porous graphitic carbon nanosheets uniformly embedded with carbon-encapsulated Fe nanoparticles
Fe_2O_3/GS	Fe_2O_3/graphene sheets
FeS_2/rGO	FeS_2 microspheres anchored on rGO
G@MoS_2-C	MoS_2 encapsulated in carbon and coupled on graphene sheets
GAMs	graphene aerogel microlattices
g-C_3N_4	carbon nitride
G-CNF film	carbon nanofiber-stabilized graphene aerogel film
G-Co_3O_4	graphene-embedded Co_3O_4 rose-spheres
GF separator	glass fibers separator
GF	graphene fiber
GNR	graphene nanoribbons
GO	graphene oxide
H-3DRG	heteroatom-doped edge-enriched 3D rivet graphene
HAADF–STEM	high-angle annular dark-field scanning transmission electron microscopy
HAH	hydroxylamine hydrochloride
HER	hydrogen evolution reaction
HG	hydrogenated graphite
HIP	hot isostatic pressing
hnp-G	hierarchical nanoporous graphene
HOPG	highly oriented pyrolytic graphite
HPC-BMS	hierarchical porous carbons with different size of pores (-B, -M, S, meaning big, medium, and small, respectively.)
HPGN	layered porous graphene nanoparticles
HR-TEM	high-resolution TEM
I_D/I_G	The ratio of D-band and G-band in the Raman spectroscopy
ITO	indium tin oxide
K	thermal conductivity
LCGO	liquid crystalline graphene oxide
LDH	layered double hydroxide
LEG	light-emitting diode
LIBs	lithium-ion batteries
LIC	lithium-ion capacitors
LMA	lithium metal anode
LMB	lithium metal battery
LMO	lithium transition-metal oxide
LOG	laterally oriented graphene
LPCVD	low-pressure CVD
LPM-3D Rebar GF	3D rebar GF prepared via a loose powder metallurgy templates method
LSG	laser scribing graphene
MBE	molecular beam epitaxy
MG	MoS_2-reduced graphene oxide

ML	monolayer
MMT	montmorillonite
MnO_2/e-CMG	graphene–MnO_2 composites
MOF	metal–organic framework
MoS_2/G	MoS_2/graphene
MO_x	the transition metal oxides
MS	molten salt
MS_2	metal disulfides
MS_x	transition metal sulfides
NCS-SG	SG on the inner surface of nano-structured Cu Scaffold
NDG/MoS_2/NDG	nitrogen-doped graphene/MoS_2/nitrogen-doped graphene
NG	nitrogen-doped graphene
Ni_3Fe/N-C	Ni_3Fe nanoparticles embedded in porous nitrogen-doped carbon sheets
NiCo-LDH	NiCo-layered double hydroxide
NiO NS/graphene	NiO nanosheets anchored on the graphene through Ni—O—C bonds composites
NiO/GF	NiO microspheres loaded on graphene foam
NiS/GNS	graphene nanosheets decorated with NiS
NiS_2@G	NiS_2@graphene
N-MG-600	N-doped nanoporous graphene synthesized at 600 °C
NO-3DG@CNC	nitrogen and oxygen co-doped 3D nanoporous duct-like graphene@carbon nano-cage hybrid films
NO-3DG@CNCs	N, O co-doped 3D nanoporous graphene@carbon nanocages
NO-3DNG	N, O co-doped nanoporous graphene
NPC	nanoporous Cu
NPs	nanoparticles
NRR	nitrogen reduction reaction
NS-800	3D N, S co-doped nanoporous graphene heated at 800 °C
NSG	nitrogen and sulfur co-doped graphene
NSP750	N, S, P tri-doped 3D nanoporous graphene obtained at 750 °C
NW	nanowire
OER	oxygen evolution reaction
OMFLC	N-doped ordered mesoporous few-layer carbon
ORR	oxygen reduction reaction
PAM	polyacrylamide
PAN	polyacrylonitrile
PANI	polyaniline
PCCF	porous cellular carbon framework
PDA	polydopamine
PECVD	plasma-enhanced chemical vapor deposition
PEDOT	poly(3,4-ethylenedioxythiophene)
PF	phenol-formaldehyde

PG	porous graphite
PIP13-FSI	*N*-methyl-*N*-propylpiperidinium bis(fluorosulfonyl)imide
PMTs	powder metallurgy templates
PP separator	polypropylene separator
PPy	polypyrrole
PPy/PG	PPy-coated porous graphene
PrGO	partially reduced graphene oxide
PTh	polythiophene
PVA	polyvinyl alcohol
PYR14-FSI	*N*-butyl-*N*-methylpyrrolidinium bis(fluorosulfonyl)imide
QD	quantum dot
QHE	quantum Hall effect
rGO	reduced graphene oxide
rGO@p-FeS_2@C	porous FeS_2 nanoparticles anchored on the surface of rGO and coated by carbon layer
rGO@ReS_2@N-C	ReS_2 nanosheets are confined in 2D-honeycombed carbon nanosheets that comprise an rGO inter-layer and a N-doped carbon coating-layer
RHE	reversible hydrogen electrode
RPECVD	remote plasma-enhanced CVD
RT	room temperature
SAED	selected area electron diffraction
SANi-NG	single-atom (SA) Ni doping on nitrogen-doped graphene frameworks
Sb/rGO	Sb-decorated rGO composite
Sb@NS-3DPCMSs	Sb@C nanoconfined nitrogen-sulfur co-doped 3D porous carbon microspheres
SCG	SEI-coated graphene
SEAD	selected area diffraction
SEASA	solvent-evaporation-assisted self-assembly
SEI	solid electrolyte interphase
SEM	scanning electron microscope
SG	stacked graphene
SG	sulfur-doped graphene
SHG	stereoscopic holes over the graphitic surface
SIBs	sodium-ion batteries
SiC	silicon carbide
Sn/NS-CNFs@rGO	ultra-small Sn nanoparticles encapsulated in N, S co-doped CNFs sheathed within rGO scrolls films
Sn@G-PGNWs	Sn nanoparticles encapsulated with graphene shells of about 1 nm
Sn-Co-G	Sn-Co nanoparticles decorated rGO composites
Sn-G	Sn nanoparticles decorated rGO composites
SPS	spark plasma sintering
SSA	specific surface area

STEM	scanning transmission electron microscopy
TBOT	tetrabutyl titanate
TEM	transmission electron microscope
UHVCVD	ultrahigh-vacuum CVD
V	voltage window
v-ReS_2	vertically aligned ReS_2 nanosheets
v-ReS_2/rGO	ReS_2 nanosheets vertically aligned on reduced graphene oxide
WGC	wrinkled graphene cage
XPS	X-ray photoelectron spectroscopy
yolk-shell CoS_2@NG	N-doped graphene-coated yolk–shell CoS_2 spheres
YS-γ-Fe_2O_3@G-GS	yolk–shell γ-Fe_2O_3@graphene
ZGNRs	zigzag graphene nanoribbons

1

Graphene-Based Materials: Structure and Properties

Xiaoyang Deng[1,2] *and Yue Li*[1]

[1] *Tianjin University, School of Materials Science and Engineering and Tianjin Key Laboratory of Composites and Functional Materials, 135 Yaguan Rd., Jinnan District, Tianjin 300350, P.R. China*
[2] *Taiyuan University of Technology, Institute of New Carbon Materials, School of Materials Science and Engineering, P.R. China*

1.1 Introduction to Carbon Materials

Carbon materials have played important role in human society due to their extremely widespread applications, as shown in Figure 1.1. For example, while carbon black was used as paint, charcoal was as a heat source according to historical materials as early as the legend of Yao and Shun. Graphite is one of the most important carbon materials with numerous functions, including as electrodes in casting/stamping/pyrometallurgy processes, in powder form as pencil lead and polishing powder, as high-quality blocks in nuclear reactors, and as refractory materials for crucibles and molds. Diamond is the hardest three-dimensional carbon material. The rare, natural form of diamond is usually used in jewelry, while the synthetic form is used in cutting tools, infrared window materials, and abradants. In addition, carbon black is an important reinforcement material for tires in the development of automobiles. Conductive carbon black is important as a conductive additive in electrode production. Carbon fibers have been a star material in their use as additive-reinforcement materials in recent decades. For example, carbon-fiber-reinforced composite materials are widely used in aircraft body parts and aerospace field. In automobiles, carbon-fiber-reinforced carbon materials can be used in brakes production, while the motor-body manufacture is a promising application for carbon-fiber-based materials. In other fields, carbon-fiber-reinforced materials can be used to fabricate fan blades for wind power generation and in sports equipment. Some examples of applications of carbon materials are illustrated, but listing every application is not possible here due to the innumerable fields where they are used.

With the present rapidly rising world population and industrialization, energy demand has led to rigorous energy-sources consumption and environmental

Templated Fabrication of Graphene-Based Materials for Energy Applications, First Edition.
Edited by Chunnian He, Naiqin Zhao, and Junwei Sha.

Figure 1.1 Typical carbon materials, such as charcoals, pencil lead, diamond, and carbon black–reinforced tires. Source: Pixabay.com. Reproduced with permission of Pixabay.

pollution problem. Hence, the development of sustainable and clean energy technologies is a great challenge for human society, and the promising solutions are exploring solar/wind/tidal energies. Although these energy sources are renewable and clean, the highly intermittent feature makes them necessarily be coupled with the energy storage systems. On the other hand, the coming electronic and information age also requires high-performance energy storage equipment. Lithium-ion batteries and supercapacitors are the most widely used energy storage devices in industry and daily life – to name a few, electric vehicles, portable electronic equipment, and power station. Active carbon and graphite are used as active materials in the electrodes of supercapacitors and lithium-ion batteries, respectively; conductive carbon black is a commonly used additive to enhance the electrical conductivity of electrodes, while now carbon nanotube (CNT) and graphene are also used as conductive additives in some products.

Carbon materials are predominantly composed of carbon atoms, and they have diverse structures and properties. There are various methods for the classification of carbon materials according to different bases – e.g. the chemical bonding modes of the carbon–carbon atoms, the production process, micro/nano-texture, and time of appearance. According to the chemical feature of carbon–carbon bonding (Figure 1.2), various families of carbon materials have been defined: C—C bonds based on the sp^3 orbitals for the diamond family materials, C—C bonds based on sp^2 orbitals to construct graphite family, C—C bonds based on sp. orbitals for carbynes, and C—C bonds with hybrid orbitals, such as graphdiyne constructed by

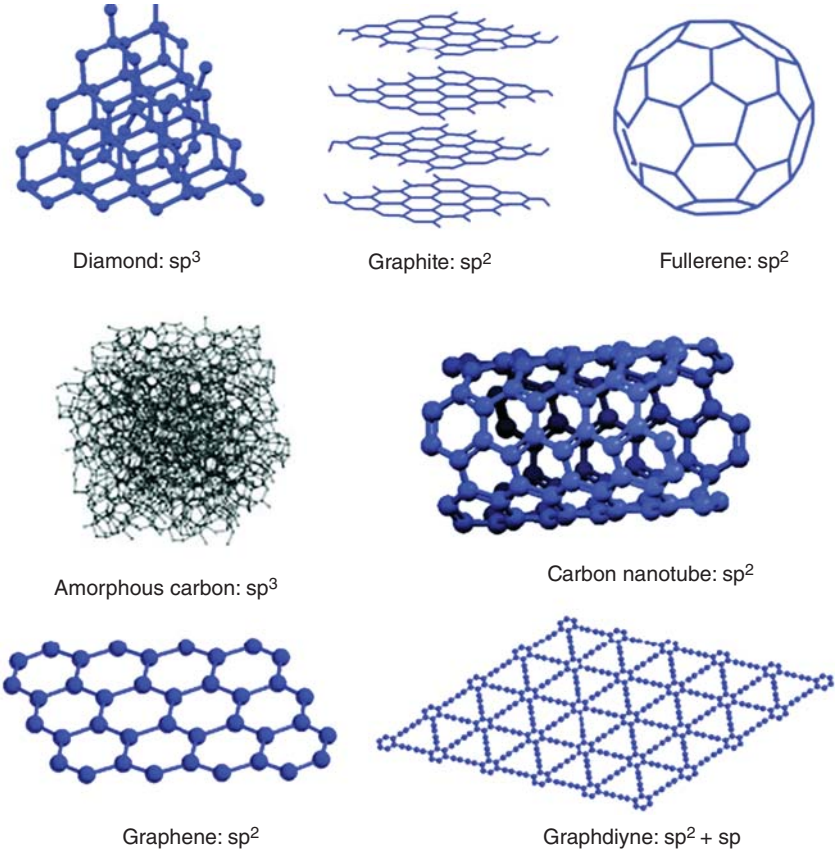

Figure 1.2 Carbon family based on carbon–carbon bonding. Source: Li et al. [1]. Reproduced with permission of Royal Society of Chemistry.

C—C bonds based on sp/sp^2 hybrid orbitals [2–5]. The most commonly used carbon materials in industry belong to the graphite family with a layered stack of carbon hexagons. Such carbon layers have strong anisotropy due to the strong covalent bonding based on sp^2 orbitals in the layers and weak bonding of van der Waals force of π electron clouds between stacked layers [4].

In the nanometer era, there have been many new members in the carbon family since the discovery of carbon nanomaterials. In 1985, zero-dimensional (0D) fullerene (C60) was first discovered with zero dimension by Smalley and coworkers [6, 7]. In 1991, the CNTs, a new one-dimensional (1D) carbon allotrope, were proposed by Iijima [8, 9]. The CNTs with various structures, i.e. thickness (single-, double-, or multi-walled), diameter, and length, have been synthesized and some types are produced on industrial scale [10]. When scaling down the thickness of graphite into nanoscale, graphene can be obtained; in other words, the monolayer graphene is the mono-unit of graphite. In 2004, graphene with two-dimensional (2D) structure was first experimentally evidenced and characterized by Geim and Novoselov, and it quickly became the most widely investigated material [11].

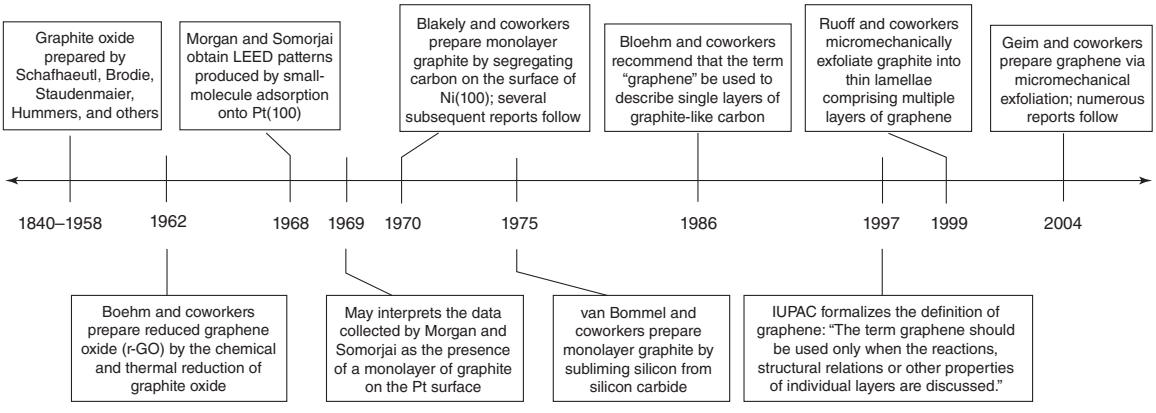

Figure 1.3 Timeline of selected events in the history of the preparation, isolation, and characterization of graphene. Source: Dreyer et al. [14]. Reproduced with permission of John Wiley and Sons.

1.2 History of Graphene

Despite a series of theoretical studies stating otherwise, as early as the 1940s, Wallace had advised that graphite might possess extraordinary electronic characteristics if its layer is isolated [12]. The term "graphene" was first proposed by Boehm et al. in 1986, who recommended that the term "graphene layer" should be used for the isolated graphitic structure constructed by only carbon atoms in one plane, which means that graphene is the most basic structure of graphite [13]. Geim, Novoselov, and coworkers used the mechanical approach to synthesize graphene in 2004, in which the highly ordered pyrolytic graphite surface was pressed against a surface of silicon wafer, and, when removed with a scotch tape, thin flakes of graphene were detected and characterized [11] (Figure 1.3). This was the first time that the existence of graphene was demonstrated through experimental evidence. In 2010, Geim and Novoselov were awarded a Nobel Prize for "groundbreaking experiments regarding the two-dimensional material graphene."

"Graphene," therefore, is defined as "an isolated single layer of carbon hexagons with sp^2-hybridized C—C bonding." In other words, as a new two-dimensional (2D) allotrope of carbon materials graphene has monoatomic thick honeycomb lattice structure (Figure 1.4a) [2, 15–18]. Hence, it can be considered as the basic building block to construct other graphitic materials, e.g. wrapped up into 0D fullerenes, rolled into 1D CNTs, and stacked to 3D graphite (Figure 1.4b) [15]. The distinctive structure and physical properties of graphene make it important for applications in technological field, such as polymer-based nanocomposites, energy storage and conversion devices (e.g. lithium-ion batteries, supercapacitors, air batteries, and fuel cells), flexible electronic and optical devices, and chemical sensors [2, 3, 19–22].

In general, some physical and chemical methods can be used to synthesize graphene, e.g. mechanical exfoliation of graphene layers from pristine graphite; chemical vapor deposition (CVD) of graphene layers on different crystals; thermal decomposition of silicon carbide (SiC); lengthwise unzipping of CNTs; exfoliation

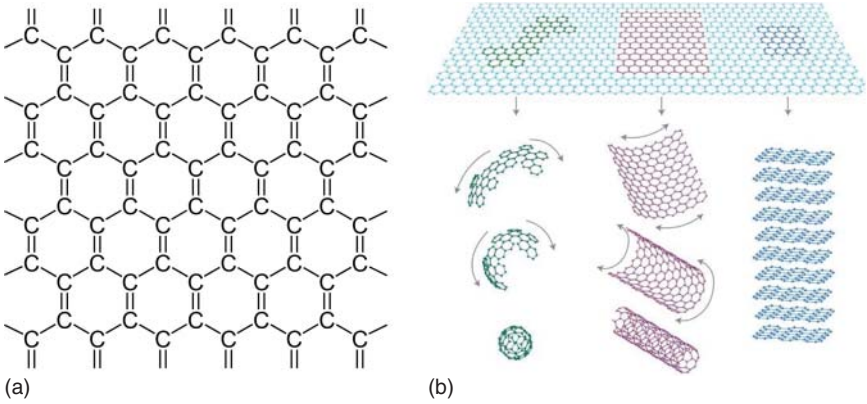

Figure 1.4 (a) Graphene structure and (b) mother of all graphitic forms. Source: Geim and Novoselov [15]. Reproduced with permission of Springer Nature.

of graphite through its intercalation compound; reduction of graphene oxides (GOs) and graphene fluoride; and organic synthesis processes [2, 23, 24]. But some methods, such as mechanical exfoliation, synthesis on SiC, and organic synthesis, exhibit difficulty in scalability and are expensive to produce, which restrict the widespread use of graphene. CVD method is unsuitable for large-scale production due to the high cost and rather low yield. The liquid-phase exfoliation process is so highly scalable and low cost that it can produce graphene in large quantities. Furthermore, although the reduced graphene oxide possesses low quality, it is still suitable for mass production due to the high yield and low cost.

1.3 Structure of Graphene

As shown in Figure 1.5a, the honeycomb lattice of graphene consists of two interpenetrating triangular sublattices, which are designated A and B. The sites of one sublattice (A) are at the centers of triangles (B) with a carbon-to-carbon interatomic length of 1.42 Å. Figure 1.5b shows the first Brillouin zone of graphene containing the high-symmetry points M, K, and K′. Each carbon atom has one *s* orbital and three p orbitals. The single s orbital is tied up with two in-plane p orbitals in the strong covalent bonding of graphene, which do not contribute to the conductivity. The remaining p orbital is oriented perpendicular to the molecular plane. This odd p orbital is hybridized to form π (valence) and π* (conduction) bands [27]. The π and π* bands touch at the K and K′ points (called Dirac points). The linear bands derived from crystal symmetry of graphene are a hallmark of graphene. This feature leads to many interesting physical properties, such as Berry's phase, half-integer quantum Hall effect (QHE), and Klein paradox. The energies of

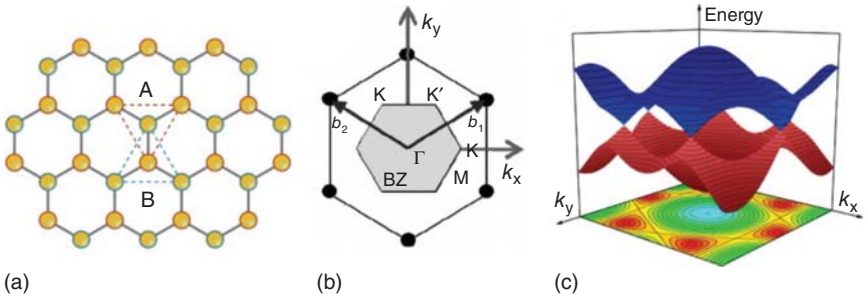

Figure 1.5 Atomic and electronic structures of graphene. (a) Graphene lattice consists of two interpenetrating triangular sublattices, each with different colors. The atoms at the sites of one sub-lattice, (i.e. A) are at the centers of the triangles defined by the other lattice (i.e. B), with a carbon-to-carbon interatomic length of 1.42 Å. Source: Rao et al. [25]. Reproduced with permission of John Wiley and Sons. (b) Reciprocal lattice of graphene. The shaded hexagon is the first Brillouin zone. (c) $\pi-\pi^*$ band structure of graphene. The three-dimensional first Brillouin zone is displayed in red and blue for the valence and conduction p bands, respectively, above the planar projection of the valence band. The six Dirac cones are positioned on a hexagonal lattice. Source: Soldano et al. [26]. Reproduced with permission of Elsevier).

the bands lie on the momentum of the charge carriers within the Brillouin zone. The constant energy contours within the linear-band approximation are circles around the K and K′ points [26]. As displayed in Figure 1.5c, the two bands meet each other and then produce cone-shaped valleys in the low-energy regime of the vicinity of the K and K′ points. In this low-energy limit, the dispersion relation of energy–momentum is linear and the carriers are seen as zero-rest mass relativistic particles. In the high-energy limit, the energy–momentum relation is changed and the distorted bands lead to anisotropy, also known as trigonal warping [26]. In addition, with stacked layers on top of each other, the electronic dispersion of graphene is changed. For example, the first-obtained bilayer graphene exhibits its own specific properties [25].

1.4 Properties of Graphene

Intrinsic (undoped) graphene is a semimetal or a semiconductor with zero bandgap. Pristine graphene possesses amazing properties, such as exceedingly high charge carriers (electrons and holes) mobility = 230 000 $cm^2\ V^{-1}\ s^{-1}$ at room temperature and an intriguing thermal conductivity of 4.84×10^3 to 5.30×10^3 $W\ m^{-1}\ K^{-1}$ at room temperature [28]. Furthermore, graphene exhibits many mechanical properties, e.g. the high mechanical stiffness of about 1 TPa [29]. In addition, graphene has an ultrahigh surface area of about 2630 $m^2\ g^{-1}$, which is significantly higher than the CNT and graphite counterparts. Besides these, we will now give a detailed account of some properties of graphene.

The existence of massless Dirac quasiparticles in graphene may be verified through the experimental observation, based on the code that the cyclotron mass was dependent on the square root of the electronic density in graphene [30, 31]. Graphene can exhibit an ambipolar electric field effect due to the zero bandgap semiconductor feature. The charge carriers in graphene can be tuned continuously between electrons and holes with concentrations as high as 1013 cm^{-2}, and mobilities of up to 15 000 $cm^2\ V^{-1}\ s^{-1}$ even under ambient conditions (Figure 1.6) [15, 30, 31]. Moreover, the low dependence of mobilities of charge carriers in graphene with temperature suggests that ultrahigh mobility would be accomplished at room temperature [32]. More importantly, when minimizing the influence of impurity scattering, mobilities in excess of 200 000 $cm^2\ V^{-1}\ s^{-1}$ could be achieved in suspended graphene [33]. The mobilities in graphene can still remain high even at a huge carrier concentration (>1012 cm^{-2}) in both electrically and chemically doped devices [34, 35]. Another measure of the electronic quality of graphene is that the QHE can be directly observed even at room temperature, which increases the temperature range for the QHE by a factor of 10 compared with previous reports [36].

Based on the Wiedemann–Franz law, the contribution of electronics is negligible for thermal conductivity in graphene; hence, the thermal conductivity (κ) of graphene is just dependent on phonon transport, namely high-temperature diffusive conduction and low-temperature ballistic conduction [37]. As early as

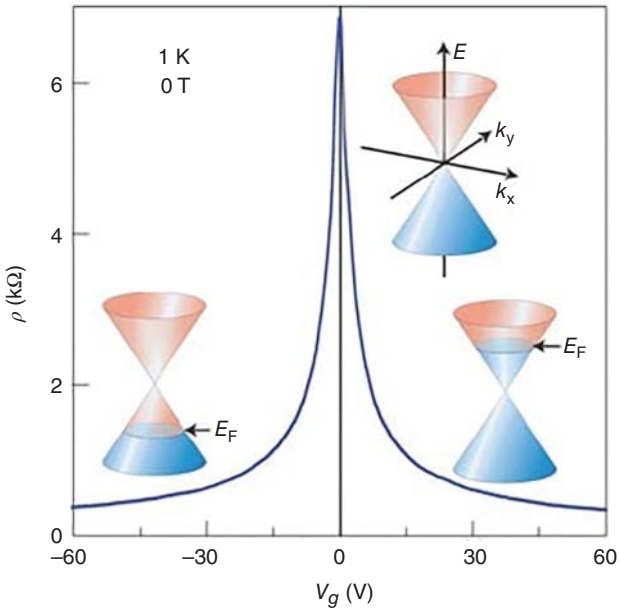

Figure 1.6 Ambipolar electric field effect in single-layer graphene. The rapid decrease in resistivity ρ on adding charge carriers indicates their high mobility (in this case, $\mu \approx 5000\,cm^2\,V^{-1}\,s^{-1}$ and does not noticeably change with increasing temperature to 300 K). Source: Geim and Novoselov [15]. Reproduced with permission of Springer Nature.

2000, the thermal conductivity of suspended monolayer graphene was predicted to be about $6000\,W\,m^{-1}\,K^{-1}$ at room temperature, much higher than that of graphitic carbon [38]. For a suspended monolayer graphene flake obtained from mechanical exfoliation, a high thermal conductivity value of about $5000\,W\,m^{-1}\,K^{-1}$ was observed through an optical measurement according to the shift of Raman G band [28].

The mechanical properties, including Young's modulus and fracture strength of monolayer graphene, have been investigated by atomic force microscopy (AFM) and numerical simulations (e.g. molecular dynamics) [39]. Particularly, the nanoindentation technique was measured using AFM to detect elastic properties and intrinsic breaking strength for free-standing monolayer graphene [29]. The results displayed that Young's modulus and fracture strength of defect-free graphene can reach 1.0 TPa and 130 GPa, respectively. The mechanical properties of some graphene materials, produced by reducing the graphene oxide, were investigated but exhibited decreased properties compared with the defect-free monolayer graphene [40–42].

The measured white light absorbances of one- and two-layered suspended graphene sheets are 2.3% and 4.6%, respectively. According to the experimental observation, the transmittance was linearly decreased based on the number of layers for n-layer graphene, and the strict linearity feature has been further demonstrated up to five monolayers [43]. This macroscopic linear dependence between the transmittance and the thickness of graphene films is intimately related to the

two-dimensional gapless electronic structure of graphene. However, when the energy of incident photons was lower than 0.5 eV, a deviation from the universal linear behavior could be observed. This deviation can be attributed to the finite temperature and chemical potential shift of the charge-neutrality (Dirac) point induced by doping [44].

1.5 Structure Defects of Graphene

To adapt to different application fields, one of the research focuses on graphene is the targeted control of its key physical and chemical properties. For this purpose, various modification methods are developed. Among them, defect engineering is considered an efficient method that can tailor mechanical, electrical, chemical, and magnetic properties of graphene [45–47]. Structural defects of graphene can be divided into two main categories. The first type is **intrinsic defects**, composed of non-sp^2 orbit hybrid carbon atoms on graphene. The carbon atomic orbital hybrid forms of change are usually caused by the absence of extra carbon atoms in the surrounding carbon six-membered rings. Therefore, obvious holes in non-six-membered carbon rings or even point or line domains can be observed in this graphene sheet at atomic resolution. The second type is **extrinsic defects**, which are generated by foreign (non-carbon) atoms covalently bonded to graphene carbon atoms. The foreign atoms (such as N, O, and B) strongly affect the charge distribution and properties of graphene [48, 49].

Specifically, **graphene intrinsic defects** can be divided into five categories: Stone–Wales defects, linear defects, single vacancies, multiple vacancies, and carbon adatoms defects. **Stone–Wales defect** is caused by simply rotating the C—C bonds to form different carbon polygon combinations (switching between pentagons, hexagons, and heptagons) without adding or removing carbon atoms. Figure 1.7 demonstrates typical Stone–Wales defects formed by rotating a C—C bond by 90° (within four neighboring hexagons that transform to two pentagons and two heptagons: $C_{6,6,6,6} \rightarrow C_{5,5} + C_{7,7}$) [50, 51]. Continuous rotation of C—C bond can be extended to linear defects consisting of paired pentagons and heptagons, as shown in Figure 1.7c. Such defects also require relatively large energy to form (~5 eV), so they can be produced by electron-beam bombardment or rapid cooling at high temperatures [52]. The existence of Stone–Wales defects significantly affects the electrical conductivity of graphene and enhances its electrochemical activity, but its strength decreases significantly [53].

Single vacancies can be considered as the simplest defects, which are formed by a missing carbon atom from continuous planar carbon six-membered ring. Similarly, on the basis of single vacancies, a continued absence of carbon atoms leads to **multiple vacancies**. Figure 1.8 displays the TEM photographs and typical atomic structures of single vacancies and multiple vacancies. The absence of dangling bonds and the steady rotation of C—C bonds make the $V_{2(555\text{-}777)}$ (7 eV) have lower formation energy than $V_{1(5\text{-}9)}$ (7.5 eV) and $V_{2(5\text{-}8\text{-}5)}$ (8 eV), so the probability of the $V_{2(555\text{-}777)}$ defect being observed by TEM is indeed greater [55, 56].

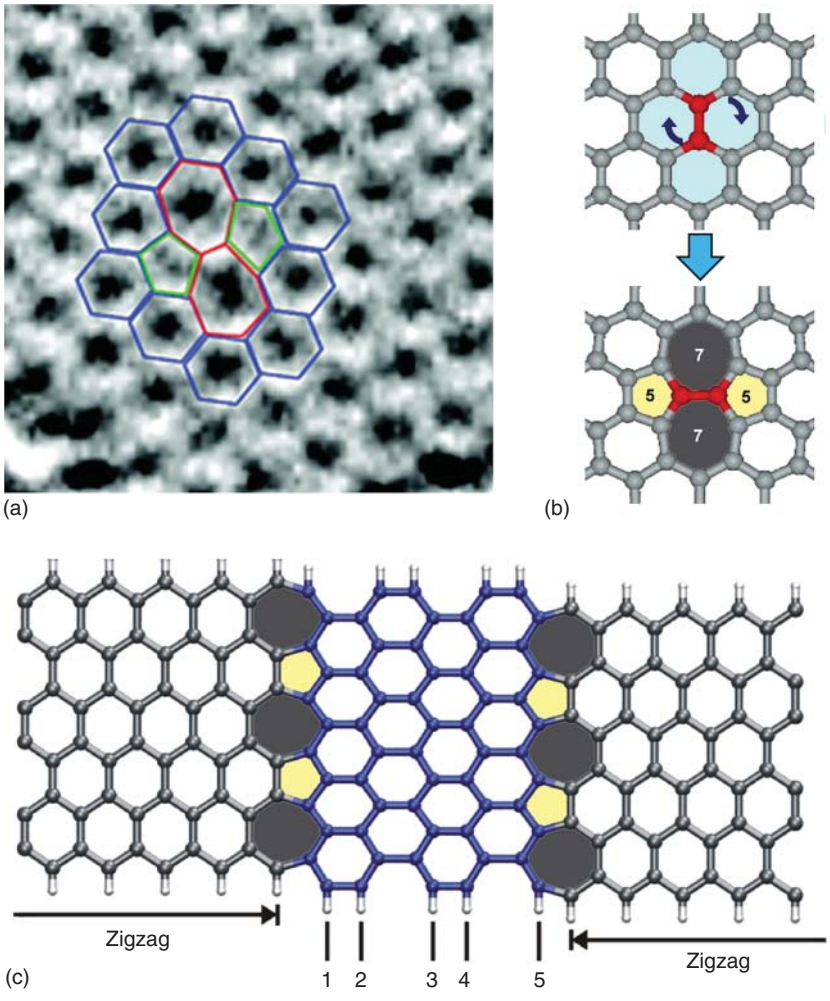

Figure 1.7 TEM image. (Source: Meyer et al. [50]. Reproduced with permission of American Chemical Society) (a) and (b) atomic structure of Stone–Wales defect in graphene by rotating a C—C bond by 90°. Source: Terrones et al. [51] Reproduced with permission of Elsevier. (c) Atomic structure of linear defect with a chain of paired rings (pentagons and heptagons). Source: Terrones et al. [51] Reproduced with permission of Elsevier.

1.5.1 Carbon Adatoms Defects

Free carbon atoms interacting with the desirable planar graphene region may destroy the original planar structure of graphene and cause sp^3-hybridization defects [57]. Figure 1.9 exhibits the spatial arrangement of carbon adatoms defects and introduction positions of free carbon atoms. The existence of carbon adatoms defects undoubtedly destroys the two-dimensional crystal structure of graphene. In particular, some defects (as presented in Figure 1.9b) directly change the orbital sp^2-hybridization type to sp^3-hybridization, which are bound to affect the electrical properties of graphene. Indeed, making such defects manageable is a big challenge for researchers.